Distribution of Megafaunal Taxa at the Pythia's Oasis Methane Seep

Emily Pinneo

University of Washington

School of Oceanography

1501 NE Boat St, Seattle, WA 98195

pinnemi@uw.edu

Running header: Distribution of Megafaunal Taxa at Pythia's Oasis

Acknowledgements

I thank Katie Bigham for mentorship with project development, analysis, machine learning, and writing, and Nikola Jensen for sharing his methods and data from Southern Hydrate Ridge. I also thank Deborah Kelley, Chief Scientist on the NSF-funded Pythias Oasis cruise (OCE 1658201) during which the imagery used in this project was collected. In addition to collecting imagery, she provided the opportunity to work on this independent thesis project, and to sail on the VISIONS cruises. I thank the Captain and crew of the R/V *Atlantis*, and the remotely operated vehicle *Jason* team for collecting photomosaic imagery. This study was supported by the University of Washington School of Oceanography and the National Science Foundation.

Abstract

Methane seeps are critical sources of productivity and habitat in the deep sea, potentially supporting major fisheries as well as contributing to nutrient cycling and carbon sequestration. Although thousands of methane seep sites have been detected, many remain unmapped and ecologically unexamined due to expense or time constraints. This study is the first survey of benthic megafauna at Pythia's Oasis, a seep with unusually high rates of venting fluid and fluid chemistry never before documented in the oceans. The fluids are thought to be sourced from overpressure in the Cascadia Subduction Zone and funneled to the site along the Alvin Canyon strike slip fault. Working from a 2019 dataset of georeferenced ROV images, this study used machine learning to increase the efficiency of image annotation and evaluated the relationship between faunal communities and substrate type. Over 22 taxa were present. The most abundant taxa included anemones, sponges, sea cucumbers, snails, corallimorphs, rockfish, and soft corals. Anemones and black corals at Pythia's Oasis may represent undescribed species. Hard and soft substrate communities are likely present, although substrate composition only explained ~16% of the variation in fauna distribution. This study demonstrates how machine learning enables scalability of image processing allowing establishment of an ecological baseline in methane seep habitats. As anthropogenic impacts on the deep sea escalate, these data are increasingly important, because they have the capacity to improve ecosystem modeling, provide the groundwork for conservation, and support sustainable fisheries management.

1. Introduction

Methane seeps are critical habitats in the deep ocean, but more research is needed to understand process linkages in these highly dynamic systems and to make informed management decisions about these essential fish habitats. They provide a variety of ecosystem services, including sequestration of teratonnes of carbon in the subsurface and nutrient cycling (Thurber et al., 2014). Methane seeps also create structure and productivity that support commercially important fisheries including rockfish, sole, and crabs like *Chionoecetes tanneri* (Grupe et al., 2015; Seabrook et al., 2019), as well as surrounding ecosystems (Levin et al., 2016). Seeps commonly represent 'hot spots' of both biomass and endemism in the deep sea (Levin et al., 2000), contributing to regional diversity.

Although these habitats may be threatened by mining for methane hydrates, trawling, pollutants, ocean acidification, and warming (Ramirez-Llodra et al., 2011) in many parts of the world, no ecological baseline for megafauna has been established. Although research to map megafauna is extensive in some locations, megafauna show wide variation between sites, making patterns difficult to generalize and detailed investigation at new sites invaluable (Seabrook et al., 2018, 2024). Understanding the structure and composition of local methane seep communities will allow us to form and test hypotheses about the drivers of megafaunal distribution, and predict distribution in adjacent areas, providing a foundation for informed, sustainable management and conservation (Cogan et al., 2009).

1.1 General Background

Methane seeps are places where methane-rich fluids diffuse out through seafloor sediments into the hydrosphere where they may be advected by water circulation (Judd et al.,

2002). Methane seeps form in areas where large amounts of methane are generated or have been generated historically, from the decomposition of buried organic matter at elevated temperatures and pressures, which causes decomposition into hydrocarbons including methane (Judd et al., 2002). Methane can also be produced biologically, when archaea break down organic matter and produce methane as a byproduct (Judd et al., 2002). Many methane seeps are highly abundant along continental shelves (Judd et al., 2002; Merle et al., 2021; Riedel et al., 2018), because high nutrient input from coastal runoff and upwelling promotes high primary productivity, high export of organic material from the surface to the deep ocean, and accretion of thick sediment deposits in subduction zone settings (Muller-Karger et al., 2005). Where sufficient concentrations of methane gas is present at conducive temperature and pressure conditions, methane is trapped inside a lattice of frozen water, forming a methane hydrate (Zatsepina & Buffett, 1997). Because methane hydrate is metastable, changes in pressure or temperature can cause methane gas to be released. The Cascadia Margin is a prime example of a region where methane seeps are abundant, with ~900 known seep locations (Judd et al., 2002; Merle et al., 2021; Riedel et al., 2018; Rudebusch et al., 2023). The compression of sediment along the Cascadia Subduction Zone accretionary margin forces methane and pore fluid out of sediment, channeling methane-rich water throughout the region through faults and porous rock (Philip et al., 2023; Rudebusch et al., 2023). Additionally, mineral dehydration reactions contribute to overpressures that drive fluid flow away from the margin.

In methane seep habitats, methane and sulfur provide energy for chemosynthetic microbes, which form the base of the food chain, as opposed to photosynthetic organisms in the surface ocean (Levin & Michener, 2002; MacAvoy et al., 2002). Different microbes may utilize aerobic or anaerobic oxidation of methane, or sulfur oxidation (Seabrook et al., 2018).

Chemosynthetic bacteria provide food for and enter into symbiotic relationships with other fauna, including vesicomyid clams and tubeworms (Boss & Turner, 1980; Childress et al., 1991). The impact of this productivity is not limited to the deep ocean or the localized area immediately surrounding the seep. Bubble plume emissions extend productivity and chemical components upwards and outwards into the water column, where organic matter may support various microbial and planktonic species (Levin et al., 2016). Seeps also provide food directly for mobile predators (MacAvoy et al., 2002), including fishes that travel across the water column and crabs that travel across the seafloor. In addition to exporting nutrients and energy to additional habitats in the ocean, many of these mobile predator species are commercially harvested. Rockfish and Sole are two examples of commercially fished species that utilize methane seep habitat (Grupe et al., 2015). *Chionoecetes tanneri* crabs are another commercially harvested species that have been found to derive significant nutrition from methane seep bacteria, both via observations of its foraging behavior and examination of gut taxa and assimilated biomarkers (Seabrook et al., 2019). The species also migrates along the seafloor, possibly moving to shallower depths with maturity, as well as migrating to form spawning aggregations (Doya et al., 2017; Keller et al., 2012), transporting energy and organic matter to new ecosystems.

Additionally, the seep environment creates physical structure that provides habitat. Chemosynthesis can cause the precipitation of significant calcium carbonate as a byproduct, forming bioherms and extensive carbonate substrates (Teichert et al., 2003). In addition to sequestering carbon, this process also provides a hard substrate for animals to colonize. Dissolution of methane hydrate deposits in the subsurface commonly results in formation of collapse zones or pockmarks in the sea floor. As buoyant methane hydrate-encased bubbles rise towards the surface, hills and hummocks also form (Suess et al., 1999; Suess, 2014; Cordes et

al., 2010). Bacterial mats, corals, snails, clams, and tube worms provide additional complexity in habitat and substrate. These dynamic environments create habitat heterogeneity that supports a diversity of organisms, including commercially fished species.

1.2 Factors that Impact Taxa Distribution

Substrate and or habitat-building species are a useful predictor of methane seep communities within a particular site: Johnson et al. (2023) found distinct megafaunal communities associated with clams in soft sediment and mussels in hard carbonate substrate. However, wide variation of megafaunal communities and habitat building species between sites can complicate the generalization of these observations. A survey of three methane seeps along the Cascadia margin found distinct bacterial communities at each location, which may play a role in structuring unique megafaunal communities (Seabrook et al., 2024). Another survey of eleven sites along the Cascadia Margin found regional trends and commonalities in microbial diversity, but also noted a high diversity of megafauna that varied between sites, including different sites characterized by vesicomyid clams, Siboglinidae tube worms, and or gooseneck barnacles. Some sites had a wide variety of corals, sponges and anemones while others did not (Seabrook et al., 2018).

Another important predictor of fauna distribution is the location, volume, and chemistry of fluid flow through the sediment. This can directly impact the distribution of habitat building species, including chemosynthetic bacteria and clams, as well as substrate. Bacterial mat, and consequently authigenic carbonate, are considered indicators of fluid flow at methane seep sites (Treude et al., 2003), because their distribution is shaped closely by fluid flow. In Monterey Bay, vesicomyid clams were only found where pore water contained detectable sulfide. Additionally, specific species of vesicomyid clams appeared to specialize in different sulfide concentrations,

and were partially segregated into zones of decreasing sulfide flux moving away from the seep (Barry et al., 1997). In a study of the Blake Ridge Diapir off the east coast, Wagner et al. (2013) also reported a 'bulls-eye' pattern of vesicomyid clams around the location of fluid flow, with mussels at the center.

A variety of factors, including oxygen concentrations and depth, may have a significant impact on methane seep communities on a broader scale as well. Oxygen concentrations and depth are commonly related, where oxygen concentrations decrease to a minimum mid-water column due to decomposition below the photic zone, then increases slightly due to the circulation of deep-water masses. Methane seeps located within oxygen minimum zones (OMZs) may have less background fauna compared to seeps outside of OMZs, possibly because some taxa found at methane seeps may be specialized for reducing, low oxygen environments that background fauna cannot tolerate (Levin et al., 2010). Additionally, OMZs may place an upper depth limit on the dispersal of certain deep sea animals, including tube worms, with a planktonic stage (Seabrook et al., 2024). Methane seeps at greater depths are more likely to have a greater degree of endemism, (Levin et al., 2000), which may be due to a scarcity of other food sources in the deep sea limiting predation (Carney, 1994)

1.3 Study Objectives

This study used high-definition imagery from the novel Pythia's Oasis methane seep site to investigate the distribution of benthic megafauna and examine what environmental factors may be related to taxa distribution. Specifically, the aims were to 1) characterize seep taxa to the lowest possible taxonomic level, 2) quantify macrofaunal abundance, density, and distribution across the site, and 3) examine whether taxa distribution could be predicted by substrate type, both for individual taxa and for communities of taxa.

2. Methods

2.1 Study Site

Pythia's Oasis is a methane seep with flow characteristics and chemistry unlike any other seep yet found in the world's oceans (Philip et al., 2023). Discovered in 2014, the site lies on the continental slope near the Cascadia Subduction Zone, 80 kilometers west of Newport, Oregon, at about 1,000 m water depth. The main orifice has been venting continuously since its discovery and compared to other seeps, the rate of fluid flow is orders of magnitude higher, at about 10 - 30 cm/s. Fluid temperatures reach the highest observed at any seep site of 12.6°C, 4 times above ambient temperatures (Philip et al., 2023). The chemistry of the site is also unique, venting fresh, highly reduced fluids. Isotopic data indicates that the fluids may be sourced at or near the plate boundary (Philip et al., 2023). The extremely high continuous emission rates and proximity to the Alvin Canyon Fault likely reflect significant fluid transported to the seep along a fault. Philip et al. (2023) reported four distinct locations of bubble plumes using hydroacoustic surveys, at least two of which have been active from 2014-2025 (Kelley pers com). Pythias has been imaged three times with an ROV, with the discovery dive made by the Canadian Scientific Submersible Facility vehicle *ROPOS*.

2.2 Data Collection

A seafloor photographic survey was conducted on September 23, 2019 using the ROV *Jason* (J2-1227) onboard the R/V *Atlantis* (cruise AT42-17) as part of the Kelley-lead NSF-funded project "Collaborative Research: Pythia's Oasis - Access to Deep Subduction Zone Fluids." The survey was focused around the primary venting orifice. The total area surveyed was roughly 68 by 75 meters. The ROV took images with a downward facing camera roughly every

20 seconds as it moved along the track lines (Fig. 1). The ROV maintained a distance of about 1-2 meters above the seafloor, with slight variations, and the altitude, geolocation, and timestamp of each image was recorded (Fig. 1). The camera was located underneath the ROV, at the same height as the navigation sensors. About 4,000 still images (5968 x 3352) were collected, as well as continuous HD video. A full record of the ROV navigation files and imagery may be provided upon request to Deborah Kelley (dskelley@uw.edu). Bathymetry data were also collected in 2019 by the autonomous underwater vehicle (AUV) Sentry, at 0.25-meter resolution (Fig. 1).

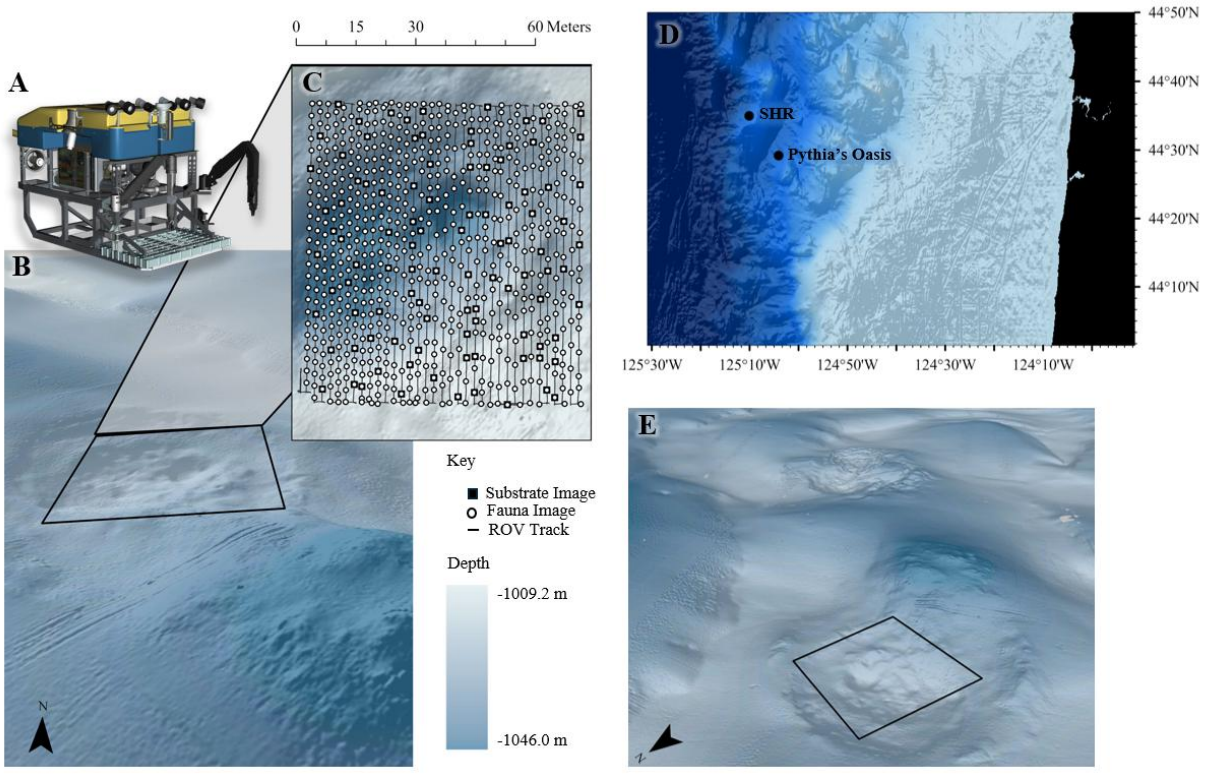

Fig. 1: Map of study site. A) An image of ROV *Jason*, credit to Woods Hole Oceanographic Institution. B) A 3D visualization showing the bathymetry at and surrounding the study site, with the survey area located with a black square. C) A survey map showing 2D bathymetry, ROV track lines, and the location of images annotated for fauna and sediment. Images annotated for fauna are indicated with a white circle, and images annotated for sediment are indicated with a black square. D) A regional view of the bathymetry, and the locations of Pythia's Oasis and Southern Hydrate Ridge relative to Oregon coast. E) A 3D visualization of Pythia's Oasis that is not oriented with North pointing up, to show details of the surrounding bathymetry. The black square again indicates the location of the survey area.

2.3 Machine-Learning Assisted Fauna Annotation

Machine learning was used to increase the efficiency of image labeling and taxonomic identification following the methodology of Bigham & Carter (2026). To select images for annotation, every fourth image from the full set of 4,000 was selected to minimize overlap (Fig. 1). The location of each image was plotted in ArcGIS Pro to identify places where images were clustered together and another 80 overlapping images were removed. Images that were not in line with other images in the same row were preferentially removed. Each image remaining in the final dataset was examined in order of timestamp and any further images with an overlapping field of view were removed. The final annotated dataset for fauna in this study included 714 images. At least every other image in the dataset (in chronological order) was annotated.

Initially, predictions were run on a subset of 100 images using the Fathomnet 315K model, an object detection model created by the Monterey Bay Aquarium Research Institute as a general identification tool for deep sea fauna (Barnard, 2018; Barnard et al., 2025). To avoid overtraining on poor quality or dark images, the initial 100 images were manually selected to include a variety of different taxa in optimal lighting and clear focus for the first iteration of the model. Then, the predicted annotations were corrected in Roboflow by manually removing incorrect bounding boxes, adding missed bounding boxes, adjusting the fit of predicted bounding boxes, and recategorizing annotation labels. A localized object detection model was fine-tuned using the corrected annotations and YOLO v12 (Redmon et al., 2016). The localized model was then used to annotate additional images, which were corrected again by hand, and all annotated images were collected to train a new model, which was used to make predictions for the final

dataset. All machine learning model training was conducted using a desktop computer with a RTX GeForce 4090 GPU.

Fauna were identified to the lowest possible taxonomic level. Taxa classes with 100-5,000 annotations were labeled major classes (Fig. 2), and taxa classes with less than 100 annotations were labeled minor classes (Fig. 3). Major classes, from largest to smallest, included sponges, small light pink anemones, *Scotoplanes*, gastropods, corralimorphs, rockfish, ctenophores, mysids, brittle stars, soft corals, large anemones, crabs, large sea pens, small dark anemones, eelpouts, sea stars, and black corals. Minor classes, from largest to smallest, included hagfish, hermit Crabs, stalked Anemones, nudibranchs, deep sea sole, sea cucumbers, deep sea skates and unknown Corals. Some initial classes used in model training were removed or combined. Visually distinct animals were sometimes grouped during annotation to avoid small classes (Fig. 4). Bathysiphon present at the site were not annotated because they were extremely small, numerous, and cryptic, making counts unreliable and time consuming. Vesicomyid clams were incompletely annotated due to time constraints and instead were removed from fauna annotations and annotated as a substrate type. Mysids and Ctenophores were also removed from further analysis, because they were primarily in the water column, so location data were not appropriate for this seafloor study.

Overestimates and underestimates of each class may have occurred due to solely image-based analysis. Dead vesicomyid clams and snails were impossible to distinguish from living clams and snails if they were upright and the shells were intact. Both clams and snails appeared to either burrow into or be covered by sediment in some cases, which could have hidden additional animals. Hermit crabs were impossible to distinguish from snails when they retreated into their shells. Crabs were observed to hide under rocks and anemones, potentially obscuring

some individuals from view during the survey. Lastly, small pink anemones commonly grew on snail shells, possibly obscuring some snails from view. Visually distinguishable dead clams, crabs and snails were excluded from biological analysis and were instead recorded as the substrate type shell rubble.

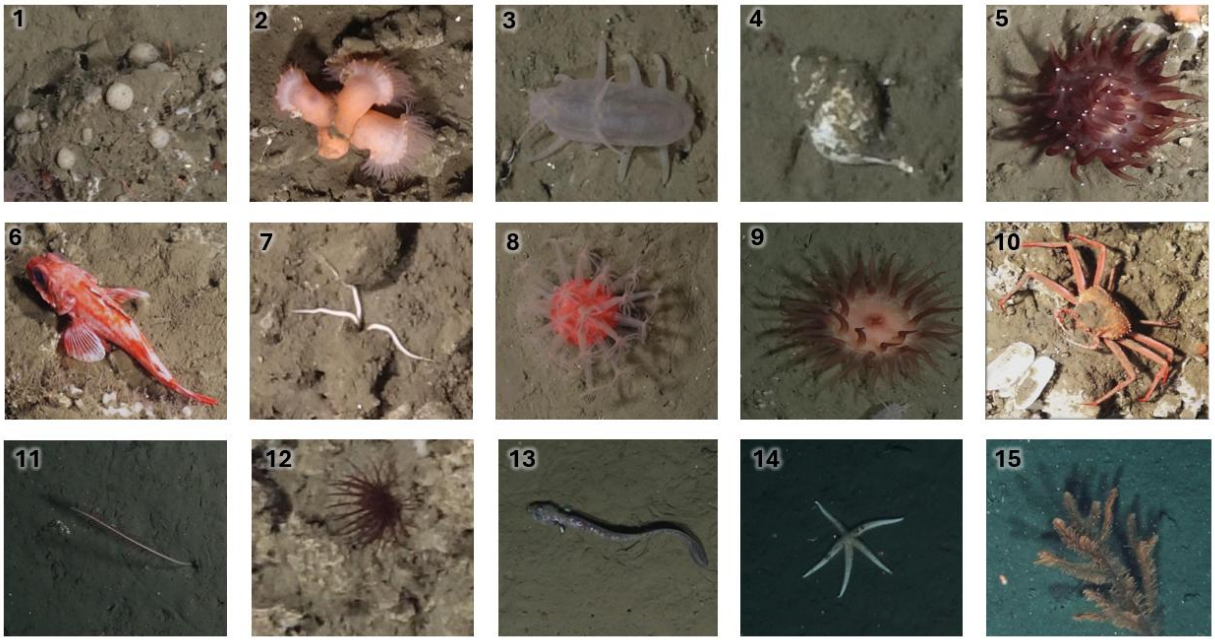

Fig. 2: Examples of the 15 major taxa classes at Pythia's Oasis, in order of annotation counts from left to right. The taxa classes are 1) sponges, 2) soft corals, 3) *Scotoplanes*, 4) gastropods, 5) corralimorphs, 6) rockfish, 7) brittle stars, 8) soft corals, 9) large anemones, 10) crabs, 11) sea pens, 12) small dark pink anemones or tubeworms, 13) eelpouts, 14) sea stars, and 15) black corals.

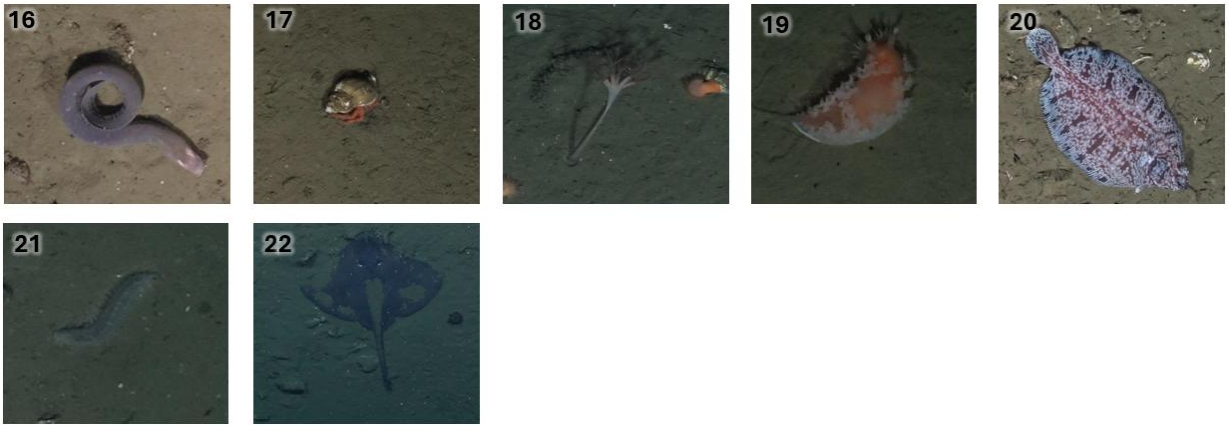

Fig. 3: Examples of the 7 minor taxa classes at Pythia's Oasis, in order of annotation counts from left to right. The order is continued following #15 in figure 2. The classes represented are 16) hagfish, 17) hermit crabs, 18) stalked anemones, 19) nudibranchs, 20) deep sea sole, 21) sea cucumbers, and 22) deep sea skates.

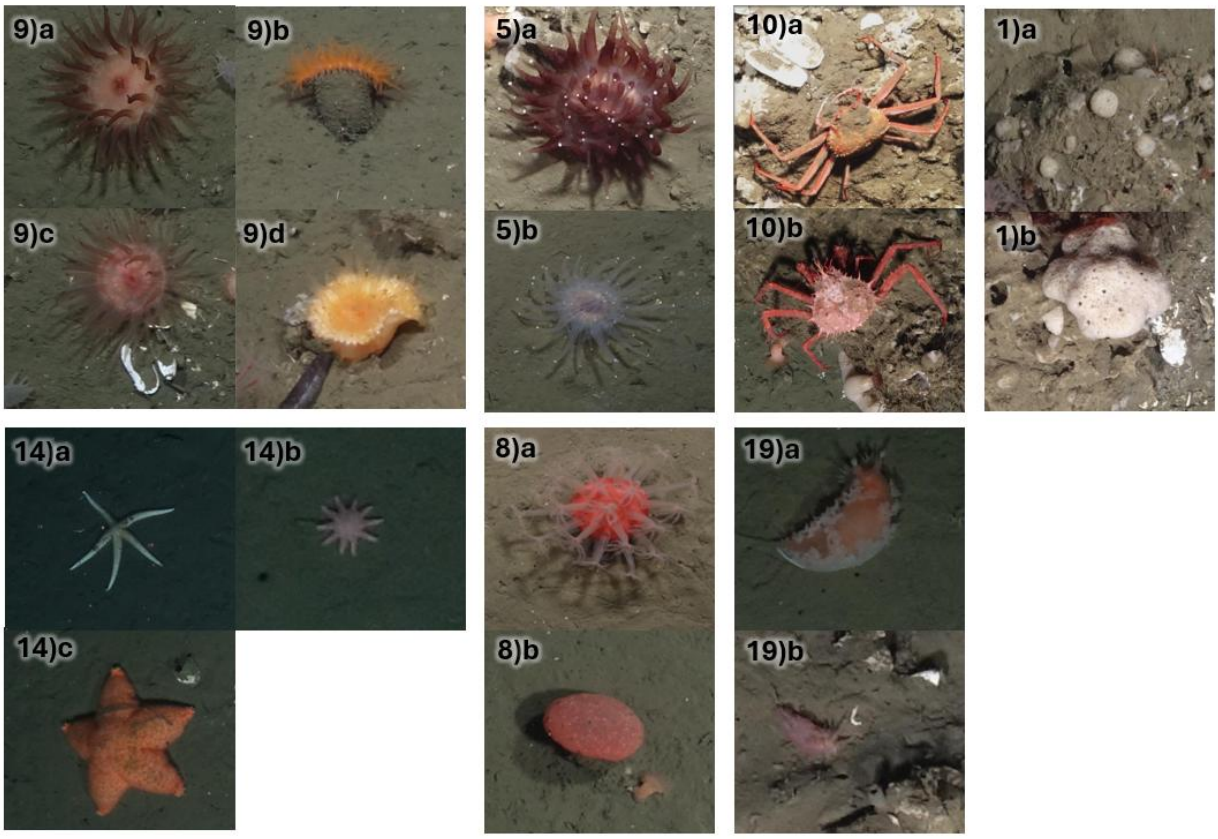

Fig 4: Examples of the variability within taxa classes. Numbering is consistent with the classes shown in Figures 2 and 3, with a, b, c, etc. indicating different visually distinct animals within the same class.

2.4 Fauna Normalization

To normalize fauna counts, fauna annotations were transformed into abundance per square meter in Excel. Scale (in meters per pixel) was calculated for each annotated image using:

$$Scale = \frac{\left(\frac{a \sin(A)}{\sin(B)}\right) * 2}{w}$$

Where a represents altitude, A represents the angle of the camera relative to vertical, B represents the angle that forms between the sediment and the direction of view, and w represents the width of the image in pixels. A and B were previously calculated by Ocean Observatories Initiative research scientist Mitch Elend while creating a photomosaic of the site, using an ROV weight as an object of known size. Then, using the scale, each image area was calculated by:

Area = (w * Scale)* (h * Scale)

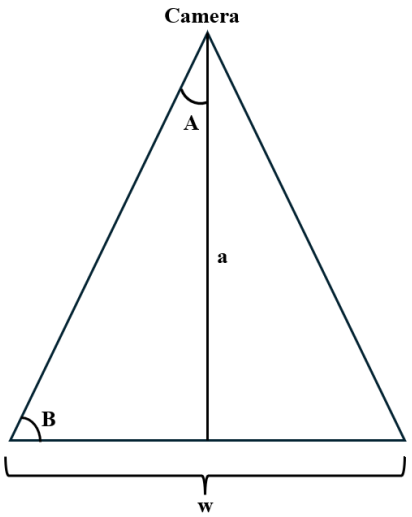

Fig. 5: Diagram showing the angles and variables used to calculate the image area.

Finally, fauna counts in each image were divided by image area. These normalized counts were then used for further analysis, as well as visualizations, in ArcGIS Pro.

2.5 Substrate Annotations

A subset of 100 images was used for sediment annotations based on methods from Bennecke & Metaxas (2017). To ensure that the substrate images were distributed across the entire site, the area was divided into 100 zones using the Fishnet tool in ArcGIS Pro, and one image was randomly selected per zone, using a Python script (Fig. 1).

Substrate images were annotated using ImageJ and Excel. A non-destructive grid was used in ImageJ to divide each image into twelve equal parts. Numbered categories were used to assess percent cover: 1 (50-100% cover), 2 (25-50% cover), 3 (5-25% cover), 4 (less than 5% cover) and 0 (not present). Each substrate type was assigned a category number for each grid cell. Substrate types included live clam bed, shell hash, authigenic carbonate, bacterial mat, mud/sand, and cobbles (Fig. 6). Grid cells that were overly dark and could not be clearly annotated were excluded. This matches the methodology used to annotate sediment at Southern Hydrate Ridge (Jensen, 2026).

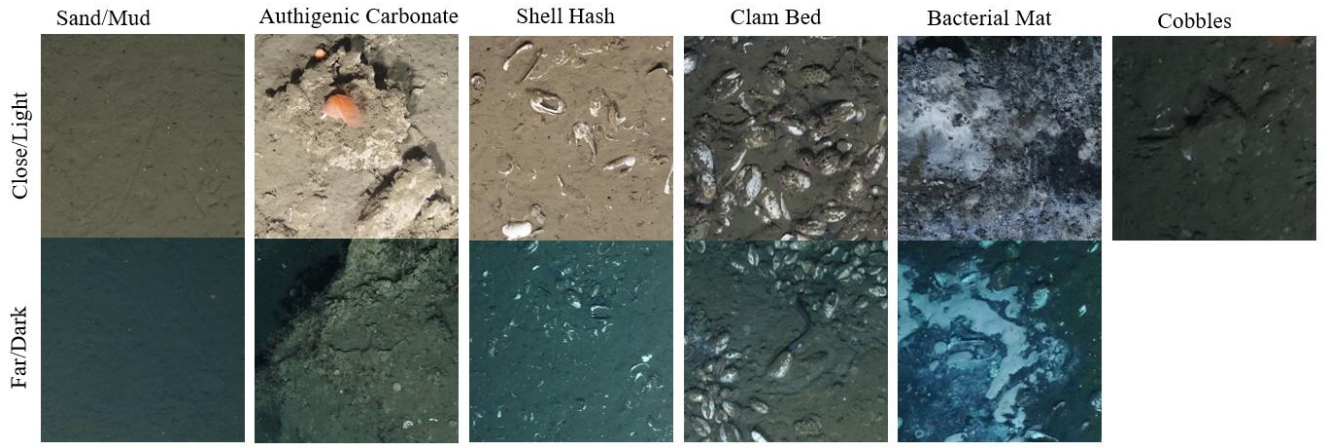

Fig. 6: Labeled examples of each substrate class. Most classes include an example that is close to the ROV camera and lights, appearing closer and warmer in color, and an example that is farther from the ROV camera and lights, appearing smaller and more blue/green in color.

2.6 Substrate Interpolation

To calculate percent cover for each image, the intermediate value for each percent cover range was assumed (i.e. for any cell marked 3, indicating 5-25% cover, 15% cover was assumed). The percent cover values were summed for each grid cell within each image by substrate type, then divided by the sum of all percent cover values to create averages for each image, using Excel.

The percent cover and coordinates in Universal Transverse Mercator (UTM) were imported into ArcGIS Pro. An Empirical Bayesian Kriging (EBK) regression prediction was used to interpolate each substrate type across the entire site. Slope and bathymetry rasters were used as explanatory variables and the percent cover data for each substrate type was used as the dependent variable in each interpolation. Minimum neighbors were set to 5 and maximum neighbors were set to 10 (Bennecke & Metaxas, 2017), the cell size was set to be the same as the bathymetry raster, and the resulting raster was snapped to the bathymetry raster.

Cross-validation data from EBK regression predictions were exported and used to calculate R squared values for each substrate interpolation. The substrate type gravel was removed from further analysis because the interpolation had a Multiple R Squared value below 0.01 (Table 1).

Substrate Type	Multiple R Squared	Adjusted R Squared	F Statistic	P Value	keep or drop
Bacterial Mat	0.03265	0.02278	3.308	0.072	keep
Authigenic Carbonate	0.218	0.21	27.31	9.77E-07	keep
Clam Bed	0.04299	0.03322	4.402	0.03847	keep
Cobbles	0.1957	0.1875	23.84	4.06E-06	keep
Gravel	0.0003235	-0.009877	0.03172	0.859	drop
Sand/Mud	0.1827	0.1743	21.9	9.20E-06	keep
Shellhash	0.1528	0.1442	17.68	5.78E-05	keep

Table 1: Table showing the R squared values for the interpolation of each substrate type.

The model builder in ArcGIS Pro was used to aggregate each regression prediction by cell factors of 1, 3, 5, 7, and 15 to allow examination of focal means. The model builder used the Aggregate (Spatial Analyst) tool with an aggregation technique of mean. This process increased the cell size by multiplying the initial cell size by the cell factor, and used the average of the smaller input cells to create a raster value for the new, larger cells. Next, all fauna annotations were uploaded as points, and intersected with the substrate interpolations and aggregations using the Extract Multi Values to Points tool (Spatial Analyst toolbox). The new, combined fauna and substrate dataset was exported as a spreadsheet for further analysis using the Table to Excel (Conversion) tool.

2.8 Statistical Analysis

Statistical analyses were conducted using PRIMER and PERMANOVA+ (Anderson et al., 2008; Clarke & Gorley, 2015). First, a square root transform was applied to the data to down-

weight the effect of highly abundant taxa. Then, a Bray-Curtis resemblance matrix was created in PRIMER. Group-average hierarchical clustering (CLUSTER) with similarity profile (SIMPROF) tests were used to identify images with similar community structures. Similarity percentage analysis (SIMPER) with a cut off of 70% was used to identify key taxa that contributed to overall community similarity within the SIMPROF groups. A non-metric multidimensional scaling (nMDS) plot was used to visualize the relationships of the SIMPROF groups.

A draftsman plot was used to determine whether each substrate interpolation, including each aggregate used for focal means, was co-correlated. All focal means aggregations with a larger scale factor than 1 were co-correlated with the highest resolution values (with a scale factor of 1) and excluded from further analysis. A Distance-based Linear Model (DistLM) and distance-based Redundancy Analysis (dbRDA) were used to determine whether environmental variables (substrate) explained variation in the fauna distribution.

4: Results

The DistLM test indicated that all substrate types explained ~16% of the variation in faunal data, with authigenic carbonate and shellhash as the most important contributors (Fig. 7). All substrate types were considered significant explanatory variables, meaning that they were included in the best solution of the DistLM.

Marginal Tests	**Variable**	**SS(trace)**	**Pseudo-F**	**P**	**Prop.**		
	Shellhash	26085	23.927	0.0001	0.033561		
	Sand/Mud	74759	73.325	0.0001	0.096186		
	Cobbles	17174	15.568	0.0001	0.022096		
	Authigenic Carbonate	86184	85.928	0.0001	0.11089		
	Bacterial Mat	3304.1	2.9415	0.0114	0.004251		
	Clam Bed	20055	18.249	0.0001	0.025803		
Sequential Tests	**Variable**	**AIC**	**SS(trace)**	**Pseudo-F**	**P**	**Prop.**	**Cumul.**
	Authigenic Carbonate	4777.3	86184	85.928	0.0001	0.11089	0.11089
	Shellhash	4754.8	24081	24.84	0.0001	0.03098	0.14187
	Cobbles	4749.3	7215.6	7.5136	0.0001	0.00928	0.15115
	Clam Bed	4744.1	6864.2	7.2123	0.0001	0.00883	0.15998
	Sand/Mud	4742.3	3573.6	3.77	0.0019	0.0046	0.16458
	Bacterial Mat	4741.4	2663.2	2.817	0.0109	0.00343	0.16801
Best Solution	**AIC**	**R^2**	**RSS**	**No.Vars**	**Selections**		
	4741.4	0.16801	6.47E+05	6	All		

Table 2: Table showing the output of the DistLM test in primer including the marginal tests, sequential tests, and the best solution. AIC = Akaike Information Criterion, SS = sum of squares, Pseudo-F = multivariate analogue Fisher's F test, p = p-value, Prop. = proportion of variation explained by each variable, and Cumul. = cumulative proportion.

The plots of substrate type and fauna density across the site highlight possible spatial overlap between substrate and fauna (Fig. 7). Sponges had the highest densities in areas where authigenic carbonate also had a high percent cover, and *Scotoplanes* had the highest densities where sand/mud had high percent cover (Fig. 7). Based on the plots, sponges may also be predicted by higher slope, although this could be co-correlated with the presence of hard substrate.

Differential distributions were apparent for some of the other fauna classes as well. Fish and crab species did not show clear patterns across the site. Gastropods had a few patches of very high density, with a consistent presence at moderate density across the rest of the site. Soft corals had a few areas of higher density, but their distribution did not match any patterns in the substrate plots. Small pink anemones had the highest densities in a rough ring in the area

between the edge and center of the study site. Clam beds also formed a ‘half-moon’ of high density around the center of the site, and bacterial mats only partially overlapped with the clam beds.

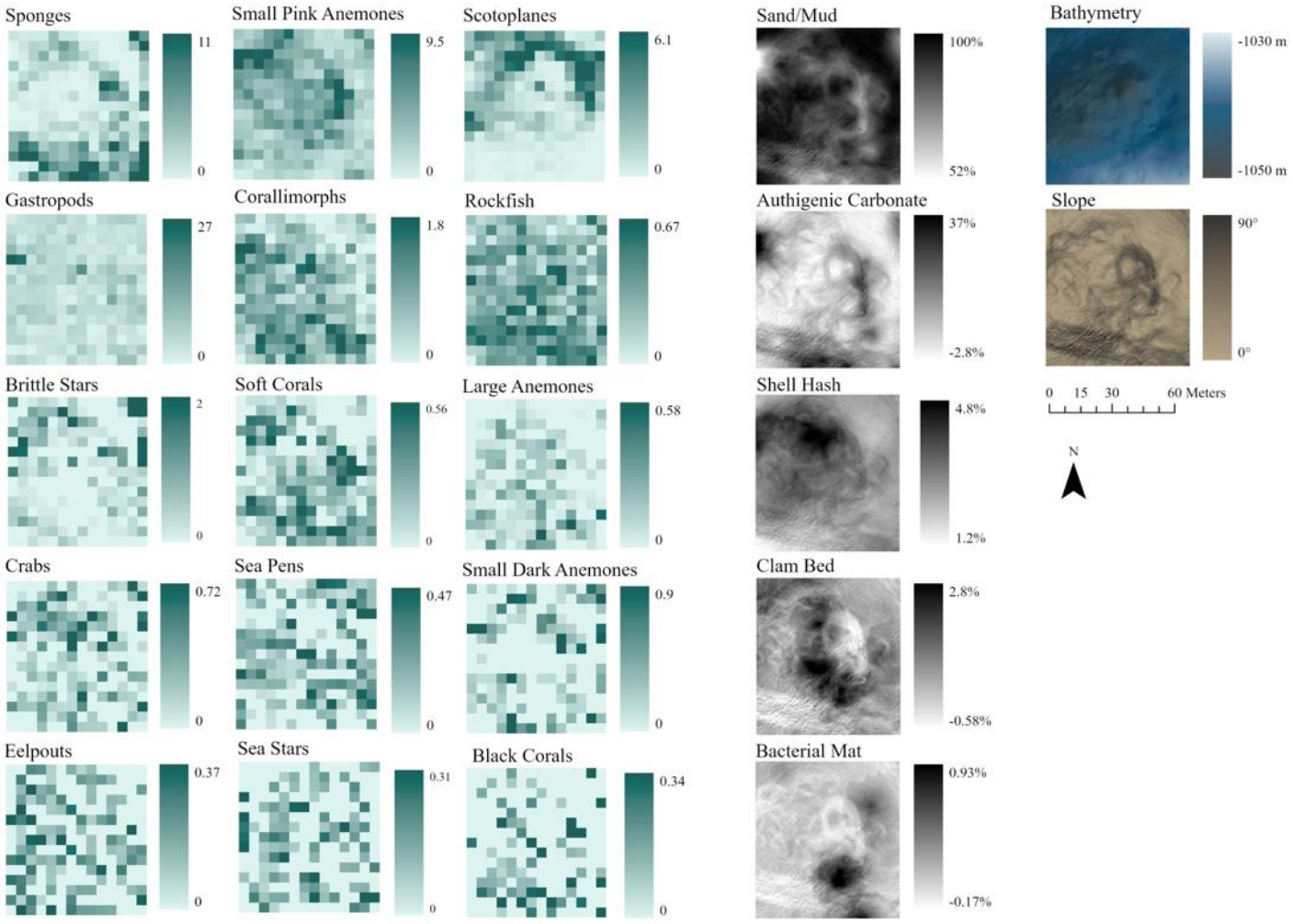

Fig. 7: Left: Heatmaps of the fauna density across the survey site. The units for fauna density are annotation count per square meter. This figure only includes the 15 fauna classes with over 100 annotations, listed in order of abundance from left to right, top to bottom. The pixel size is 5.3 meters for each fauna class, but the density scales vary.

Right: plots of substrate type, in decimal percent cover, as well as slope (in degrees) and depth (in meters) across the site. Bathymetry is reported in 0.25 meter resolution.

Three of the groups identified by the CLUSTER-SIMPROF analysis, labeled n, m and p, showed spatially distinct distributions and represented a large number of the images (Fig. 8). The three groups were primarily distinguished by the presence/density of sponges and *Scotoplanes* (Table 3). Small pink anemones and gastropods were present in all of the groups, but did not greatly contribute to differences in similarity between groups (Table 3). Results of non-metric multidimensional scaling (nMDS) delineated three distinct groups within the faunal data that aligned with the main SIMPER communities, but the stress was very high, which made the results uninterpretable (Fig. 9).

The spatial extent of each community overlapped with a different substrate type. Community n, distinguished by a high abundance of sponges, overlaps spatially with high percent cover areas for authigenic carbonate. Community m was distinguished by a lower abundance of sponges and the presence of *Scotoplanes*, and overlaps spatially with a transitional zone between authigenic carbonate and sand/mud. Community p was distinguished by very few sponges and very high densities of *Scotoplanes*, overlapping with high percent cover areas for sand/mud substrate (Fig. 8).

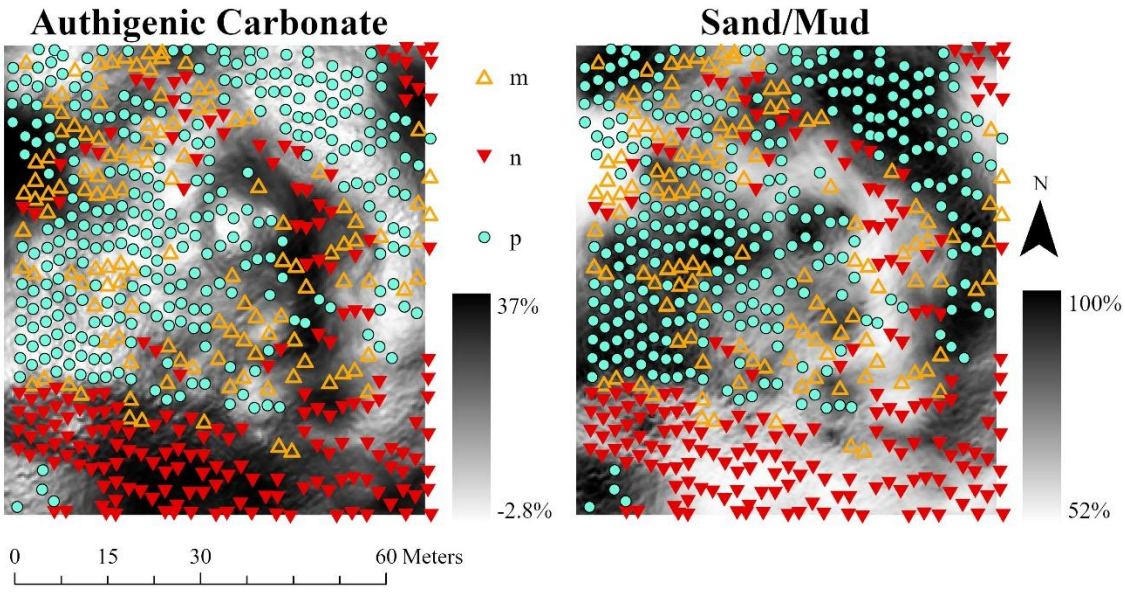

Fig. 8: Bottom: a map showing the location of each sample that was identified as one of the main SIMPER communities n, m and p, shown plotted over the substrate interpolation for authigenic carbonate (right) and sand/mud (left). The community m is represented by the outline of an upward-pointing orange triangle, the community n is represented by a downward-pointing, solid red triangle, and the community p is represented by a solid cyan circle with a black outline.

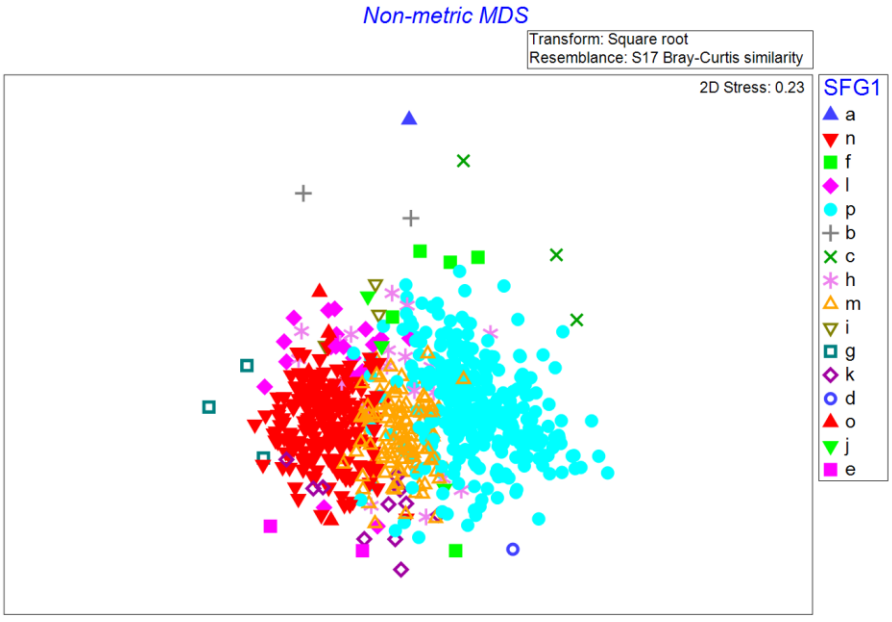

Fig. 9: nMDS plot of fauna created in PRIMER. The three communities labeled n, m and p are closely clustered and represent the majority of the data, but the stress value is too high to interpret the results.

Group	Overall Av. Sim	Taxa Class	Av. Abund	Av. Sim	Sim/SD	Contrib%	Cum.%
m	66.86	Small Light Pink Anemone	1.41	16.88	3.91	25.24	25.24
		Sponge	1.06	11.57	2.47	17.31	42.55
		Scotoplanes	1.1	11.48	2.55	17.16	59.71
		Gastropoda	0.82	9.44	2.72	14.11	73.83
n	66.74	Sponge	2.03	22.4	4.1	33.57	33.57
		Small Light Pink Anemone	1.22	12.81	2.78	19.19	52.76
		Gastropoda	0.8	8.61	2.74	12.89	65.65
		Corallimorph	0.69	7.1	1.75	10.64	76.3
p	60.51	Small Light Pink Anemone	1.18	19.42	2.93	32.1	32.1
		Scotoplanes	1.14	16.15	1.64	26.69	58.79
		Gastropoda	0.83	13.15	2.26	21.73	80.52

	Overall Av. Diss	Taxa Class	Av. Abund *n*	Av. Abund *p*	Av. Diss	Diss/SD	Contrib%	Cum.%
Groups *n* & *p*	54.59	Sponge	2.03	0.12	15.58	2.96	28.54	28.54
		Scotoplanes	0.28	1.14	8	1.53	14.66	43.19
		Small Light Pink Anemone	1.22	1.18	4.13	1.28	7.56	50.75
		Corallimorph	0.69	0.41	3.81	1.29	6.98	57.73
		Gastropoda	0.8	0.83	2.94	1.23	5.39	63.12
		Soft Coral	0.36	0.1	2.84	1.22	5.21	68.33
		Sebastolobus	0.6	0.37	2.69	1.21	4.92	73.25
	Overall Av. Diss	**Taxa Class**	**Av. Abund *n***	**Av. Abund *m***	**Av. Diss**	**Diss/SD**	**Contrib%**	**Cum.%**
Groups *m* & *n*	39.8	Sponge	2.03	1.06	7.21	1.57	18.11	18.11
		Scotoplanes	0.28	1.1	6.37	1.61	16.01	34.13
		Small Light Pink Anemone	1.22	1.41	3.69	1.35	9.27	43.39
		Brittle_Star	0.31	0.26	2.61	0.99	6.55	49.94
		Corallimorph	0.69	0.63	2.51	1.23	6.3	56.24
		Gastropoda	0.8	0.82	2.29	1.23	5.74	61.99
		Soft Coral	0.36	0.3	2.23	1.23	5.6	67.59
		Sebastolobus	0.6	0.5	1.94	1.17	4.88	72.47
	Overall Av. Diss	**Taxa Class**	**Av. Abund *p***	**Av. Abund *m***	**Av. Diss**	**Diss/SD**	**Contrib%**	**Cum.%**
Groups *p* & *m*	42.95	Sponge	0.12	1.06	8.17	2.03	19.02	19.02
		Scotoplanes	1.14	1.1	5.48	1.32	12.77	31.79
		Small Light Pink Anemone	1.18	1.41	4.29	1.3	9.99	41.77
		Corallimorph	0.41	0.63	3.65	1.3	8.49	50.26
		Gastropoda	0.83	0.82	2.99	1.23	6.96	57.22
		Sebastolobus	0.37	0.5	2.79	1.22	6.51	63.73
		Soft Coral	0.1	0.3	2.51	1.12	5.84	69.57
		Brittle Star	0.07	0.26	2.26	0.83	5.26	74.83

Table 3: Table showing the SIMPER results for the within group (top) and between group (bottom) similarity. This table only includes the results for the three most distinct groups the full results for all groups are available upon request. Overall Av. Sim = similarity of all taxa within each group, Av. Abund = average abundance, Av. Sim = average similarity, Sim/SD = similarity divided by standard deviation, Contrib% = percent contribution, and Cum% = cumulative contribution. Overall Av. Diss = average dissimilarity of all taxa within a group, Av. Diss = average dissimilarity, Diss/SD = dissimilarity divided by standard deviation, Contrib% = percent contribution, and cum % = cumulative percent.

4. Discussion

Overall, 22 different taxa were found at Pythia's Oasis, which, when accounting for variability within classes, probably represented a larger number of species. Stalked and light pink anemones at the site may be previously undescribed species, as well as large anemones and black corals. The most abundant taxa classes included sponges, light pink anemones, *Scotoplanes*, gastropods, and corallimorphs. Sponges and *Scotoplanes* in particular were key species whose abundance may indicate differential communities between hard and soft substrates at Pythia's Oasis. Substrate was primarily composed of sand/mud and authigenic carbonate.

4.1 DistLM and Substrate

Substrate explained ~16% of fauna variability, which is typical for similar methane seep studies (Case et al., 2015; Cleland et al., 2021), but it is also clear that other variables also impacted taxa distribution. To better understand faunal distribution, it would be useful to further examine the role of interspecies interactions and behavior, as well as environmental variables that include water chemistry, temperature and prevailing current direction.

The DistLM indicated that authigenic carbonate and shell hash predicted the greatest proportion of the taxa variability, with sand/mud explaining a very small proportion of taxa variability. However, these results should be interpreted with caution. The DistLM only accounted for a small amount of the overall variation in the fauna community. Additionally, sand/mud and authigenic carbonate were the two main substrate types present in the majority of the surveyed area, with bacterial mat, cobbles and clam bed occurring over a much smaller area. Sand/mud and authigenic carbonate were likely somewhat negatively correlated because of this relationship, causing sand/mud to appear much less significant in the DistLM than in actuality.

Bacterial mat, while considered significant by the DistLM, minimally explained fauna distribution. Additionally, no taxa class was strongly correlated with a high percent cover of bacterial mat. This was surprising, because bacterial mats are commonly used as a stand in for active seeping, and are typically expected to have a large impact on fauna communities (Treude et al., 2003). A spatiotemporal study at Southern Hydrate Ridge, a site about 10 km north of Pythia's Oasis, found that the same subsampling annotation method used in this study did not fully capture bacterial mat distribution (Jensen, 2026), so another method may be more appropriate for small, patchy substrate types.

Clam beds also showed very poor correlation with taxa variability. The 'bulls-eye' pattern of vesicomyid clams around the Blake Ridge seep found by Wagner et al. (2013), where clams surrounded active seepage in a ring, was not visible on the scale of the plot of substrate types (Fig. 7), despite surveying on a similar scale. Instead, there was a 'half moon' of high clam percent cover that was not centered around bacterial mats. However, the 'bullseye' pattern could be seen in some cases in individual images (Fig. 10). Clam beds occurred with high density immediately adjacent and not extending into bacterial mats, but living clams did not always form a complete ring around bacterial mats.

It is possible that a much finer scale analysis would reveal more meaningful patterns for clam beds and bacterial mats, because variation within a single image was averaged in these analyses. It would be beneficial for future studies to extrapolate the position of each annotation within each image, to more precisely characterize the area and shape of bacterial mats, and or work from annotations from the full photomosaic or a larger subset, to better delineate these differences in taxa distributions at an even finer scale.

Fig. 10: Examples of a 'bullseye' pattern of vesicomyid clams of greatest densities immediately adjacent to and surrounding bacterial mats, within the scale of a single image. Right: clams and clam shells completely surround the bacterial mat. Left: the clam bed is only present on the lower side of the bacterial mat.

The dataset includes extremely high-quality imagery, with visible indicators of bioturbation that could be used in the future to analyze animal behavior. For instance, in many cases a path of travel was evident behind clams and gastropods. Future studies could use this to quantify the mobility and travel tendencies of these animals in response to other taxa or active seep areas. As the location and volume of fluid flow likely varies over time (Carson & Screaton, 1998), this would shed light on the capacity of such fauna to respond to these changes, with potential implications for their resilience to anthropogenic impact as well.

4.2 Fauna Distributions Compared to Substrate

High sponge density appears to correlate with a high percent cover of authigenic carbonate, and high scotoplane density appears to correlate with areas a high percent cover of

sand/mud. This difference in distribution is consistent with the life history of each organism – sponges may require a hard substrate to attach to, while *Scotoplanes* feed by filtering sediment for organic particles. High brittle star density also appeared correlated with a high percent coverage of shell hash and possibly authigenic carbonate. Brittle stars were observed hiding under both of these hard substrate types, which may represent a preferred habitat.

Large anemones, corallimorphs, and corals showed some patterns in distribution, with areas of higher density, but were not well predicted by any of the study substrate categories. Future studies should investigate other factors that may predict their distribution, in order to better model their habitat and inform sustainable management. The corals in particular are likely long-lived: a soft coral species in the same genus as Pythia's Oasis corals, *Anthomastus ritteri*, does not reach full size until it is 25-30 years old (Cordes et al., 2001). Black corals were also found at Pythia's Oasis, and could have life spans ranging from hundreds to thousands of years (Prouty et al., 2011). The longevity and fragility of deep sea corals makes them particularly vulnerable to bottom trawling (González-Irusta et al., 2018), and they may be threatened with extinction unless managed appropriately.

The distribution of more mobile animals, including eelpouts, rockfish, and crabs did not show a clear spatial pattern. This was expected, because these animals move more easily and quickly and are not constrained to specific areas.

Although crab distribution was not well aligned with substrate overall, one area of high crab density correlated with the highest percent cover for shell hash. This raises the question: could crabs contribute to shell breaks and the creation of shell hash? The majority of crabs in this study likely represent the genus *Chionoecetes,* with only one individual appearing to belong to another family (probably a king crab from family Lithodidae), both of which are shown in Fig. 4.

C. tanneri crabs are known to feed on methane seep bacteria (Seabrook et al., 2019), but crab distribution at Pythia's did not appear to align with bacterial mats. *C. tanneri* have also been observed to feed on fish, annelid worms, mollusks including snails and bivalves, other arthropods, and echinoderms in shallow waters (less than 200m) near Kodiak Island, Alaska (Jewett & Feder, 1983). The full range of prey for *Chionoecetes* is wide and probably varies by location. Barry et al. (1996) stated that *C. tanneri* crabs prey on vesicomyid clams, however, this has not yet been observed at Pythia's Oasis. It would be interesting for future studies to investigate the stomach contents and foraging behaviors of *Chionoecetes* at Pythia's Oasis, as well as the response of other taxa as crab populations fluctuate over time. If crabs act as a control on habitat building species like clams, they could have a significant impact on community structure.

4.3 Community Distributions

Overall, the statistics and plots show faunal correlations between soft and hard substrate communities at Pythia's Oasis. The three main communities (n, m, and p) may represent hard (authigenic carbonate), transitional (mud and authigenic carbonate), and soft (sand/mud) substrate communities (Fig. 8). The composition of each community, and the plots of individual taxa distribution support this hypothesis: abundances of sponges and *Scotoplanes* were the main taxa that distinguished each community, and were also the taxa with density that was most closely correlated with substrate (Fig 7).

Small pink anemones and gastropods were found in all three of the main communities, but were taxa that minimally contributed to differences between those communities. This could indicate that small pink anemones and gastropods were ubiquitous across the entire site. Although the small pink anemone and gastropod distribution did not clearly align (Fig. 7), these

fauna were commonly observed in close association, with one or more small pink anemones growing on gastropods. In some cases, the small pink anemones grew so large or so numerous that they almost entirely obscured the gastropods, but the track from the gastropod's movement, or its foot or appendages were visible. As many as four small pink anemones were hosted on the same snail shell. It would be interesting for future studies to investigate whether there is a symbiotic relationship between the snails and the light pink anemones. If anemones growing on snail shells increases the energy required for the snail to move and forage, this could decrease snail fitness and impact community dynamics. Small pink anemones were also observed, more rarely, growing on other shell rubble and on clam shells, highlighting a possible requirement for hard substrates.

5. Conclusion

This study utilized high resolution bathymetry and high-definition images, coupled with machine learning, to complete the first documentation of faunal communities at the novel Pythias Oasis methane seep. Here, substrate is an important predictor of fauna distribution, especially for sponges and *Scotoplanes*, with distinct communities in soft, hard and transitional substrates. Additional research is needed to investigate the remaining variables that predict distribution at Pythia's Oasis, including the behavior of and the relationships between animals. This study demonstrates the utility of machine learning technology to process marine imagery and extract data from pre-existing collections to broaden our understanding of deep-sea ecology. Results from this investigation form a foundation for further research and modeling, which are necessary to inform sustainable management and conservation in the high productivity methane seep sites that are largely unexplored along all continental margins (Cogan et al., 2009).

6. References

Anderson, M. J., Gorley, R. N., & Clarke, K. R. (2008). *PERMANOVA+ for PRIMER:... | PRIMER-e Learning Hub*. https://learninghub.primer-e.com/books/permanova-for-primer-guide-to-software-and-statistical-methods

Barnard, K. (2018). *Fathomnet: Building the Datset*. Google Docs. https://drive.google.com/file/u/1/d/1NI42q1wCoX7Ueehyr5b3T3-tQzZ9d4Ia/view?usp=embed_facebook

Barnard, K., Liu, E., Walz, K., Schlining, B., Stout, N. J., & Lundsten, L. (2025). *DeepSea MOT: A benchmark dataset for multi-object tracking on deep-sea video* (arXiv:2509.03499). arXiv. https://doi.org/10.48550/arXiv.2509.03499

Barry, J. P., Gary Greene, H., Orange, D. L., Baxter, C. H., Robison, B. H., Kochevar, R. E., Nybakken, J. W., R, D. L., & McHugh, C. M. (1996). Biologic and geologic characteristics of cold seeps in Monterey Bay, California. *Deep Sea Research Part I: Oceanographic Research Papers*, *43*(11), 1739–1762. https://doi.org/10.1016/S0967-0637(96)00075-1

Barry, J. P., Kochevar, R. E., & Baxter, C. H. (1997). The Influence of Pore-Water Chemistry and Physiology on the Distribution of Vesicomyid Clams at Cold Seeps in Monterey Bay: Implications for Patterns of Chemosynthetic Community Organization. *Limnology and Oceanography*, *42*(2), 318–328.

Bennecke, S., & Metaxas, A. (2017). Is substrate composition a suitable predictor for deep-water coral occurrence on fine scales? *Deep Sea Research Part I: Oceanographic Research Papers*, *124*, 55–65. https://doi.org/10.1016/j.dsr.2017.04.011

Bigham, K. T., & Carter, A. (2026). A machine learning assisted method for rapidly annotating benthic megafauna in large volumes of marine imagery. *Limnology and Oceanography: Methods*, *n/a*(n/a), e70057. https://doi.org/10.1002/lom3.70057

Boss, K. J., & Turner, R. D. (1980). THE GIANT WHITE CLAM FROM THE GALAPAGOS RIFT, CALYPTOGENA MAGNIFICA SPECIES NOVUM. *Malacologia*.

Carney, R. S. (1994). Consideration of the oasis analogy for chemosynthetic communities at Gulf of Mexico hydrocarbon vents. *Geo-Marine Letters*, *14*(2), 149–159. https://doi.org/10.1007/BF01203726

Carson, B., & Screaton, E. J. (1998). Fluid flow in accretionary prisms: Evidence for focused, time-variable discharge. *Reviews of Geophysics*, *36*(3), 329–351. https://doi.org/10.1029/97RG03633

Case, D. H., Pasulka, A. L., Marlow, J. J., Grupe, B. M., Levin, L. A., & Orphan, V. J. (2015). Methane Seep Carbonates Host Distinct, Diverse, and Dynamic Microbial Assemblages. *mBio*, *6*(6), 10.1128/mbio.01348-15. https://doi.org/10.1128/mbio.01348-15

Childress, J. J., Fisher, C. R., Favuzzi, J. A., & Sanders, N. K. (1991). Sulfide and Carbon Dioxide Uptake by the Hydrothermal Vent Clam, Calyptogena magnifica, and Its Chemoautotrophic Symbionts. *Physiological Zoology*, *64*(6), 1444–1470.

Clarke, K. R., & Gorley, R. N. (2015). *Getting started with PRIMER v7*.

Cleland, J., Kazanidis, G., Roberts, J. M., & Ross, S. W. (2021). Distribution of Megabenthic Communities Under Contrasting Settings in Deep-Sea Cold Seeps Near Northwest Atlantic Canyons. *Frontiers in Marine Science*, *8*. https://doi.org/10.3389/fmars.2021.692851

Cogan, C. B., Todd, B. J., Lawton, P., & Noji, T. T. (2009). The role of marine habitat mapping in ecosystem-based management. *ICES Journal of Marine Science*, *66*(9), 2033–2042. https://doi.org/10.1093/icesjms/fsp214

Cordes, E. E., Cunha, M. R., Galéron, J., Mora, C., Olu-Le Roy, K., Sibuet, M., Van Gaever, S., Vanreusel, A., & Levin, L. A. (2010). The influence of geological, geochemical, and biogenic habitat heterogeneity on seep biodiversity. *Marine Ecology*, *31*(1), 51–65. https://doi.org/10.1111/j.1439-0485.2009.00334.x

Cordes, E. E., Nybakken, J. W., & VanDykhuizen, G. (2001). Reproduction and growth of Anthomastus ritteri (Octocorallia: Alcyonacea) from Monterey Bay, California, USA. *Marine Biology*, *138*(3), 491–501. https://doi.org/10.1007/s002270000470

Doya, C., Chatzievangelou, D., Bahamon, N., Purser, A., Leo, F. C. D., Juniper, S. K., Thomsen, L., & Aguzzi, J. (2017). Seasonal monitoring of deep-sea megabenthos in Barkley Canyon cold seep by internet operated vehicle (IOV). *PLOS ONE*, *12*(5), e0176917. https://doi.org/10.1371/journal.pone.0176917

González-Irusta, J. M., De la Torriente, A., Punzón, A., Blanco, M., & Serrano, A. (2018). Determining and mapping species sensitivity to trawling impacts: The BEnthos Sensitivity Index to Trawling Operations (BESITO). *ICES Journal of Marine Science*, *75*(5), 1710–1721. https://doi.org/10.1093/icesjms/fsy030

Goode, S. L., Rowden, A. A., Bowden, D. A., Clark, M. R., & Stephenson, F. (2021). Fine-Scale Mapping of Mega-Epibenthic Communities and Their Patch Characteristics on Two New Zealand Seamounts. *Frontiers in Marine Science*, *8*. https://doi.org/10.3389/fmars.2021.765407

Grupe, B. M., Krach, M. L., Pasulka, A. L., Maloney, J. M., Levin, L. A., & Frieder, C. A. (2015). Methane seep ecosystem functions and services from a recently discovered southern California seep. *Marine Ecology*, *36*(S1), 91–108. https://doi.org/10.1111/maec.12243

Jensen, N. (2026). *Structuring Effects of Seep-Associated Environmental Factors on the Distribution of Megabenthos at Southern Hydrate Ridge, Oregon Continental Margin*. Google Docs.

https://docs.google.com/document/u/1/d/1cS4bGnJUnysBkKikJPtqLoLSqIu6Wb6IfdkQ2uNWnko/edit?usp=sharing&usp=embed_facebook

Jewett, S. C., & Feder, H. M. (1983). Food of the Tanner Crab Chionoecetes bairdi near Kodiak Island, Alaska. *Journal of Crustacean Biology*, *3*(2), 196–207. https://doi.org/10.2307/1548256

Johnson, H. P., Miller, U. K., Salmi, M. S., & Solomon, E. A. (2015). Analysis of bubble plume distributions to evaluate methane hydrate decomposition on the continental slope. *Geochemistry, Geophysics, Geosystems*, *16*(11), 3825–3839. https://doi.org/10.1002/2015GC005955

Johnson, K., Taylor, A., Socha, A., Barkyoumb, E., Nakamura, K., Kaiser, C. L., German, C. R., Yoerger, D. R., & Van Dover, C. L. (2023). Seascape ecology in the vicinity of a Blake Ridge cold seep. *Frontiers in Marine Science*, *10*. https://doi.org/10.3389/fmars.2023.1198226

Judd, A. G., Hovland, M., Dimitrov, L. I., García Gil, S., & Jukes, V. (2002). The geological methane budget at Continental Margins and its influence on climate change. *Geofluids*, *2*(2), 109–126. https://doi.org/10.1046/j.1468-8123.2002.00027.x

Keller, A. A., Harms, J. H., & Buchanan, J. C. (2012). Distribution, biomass and size of grooved Tanner crabs (*Chionoecetes tanneri*) from annual bottom trawl surveys (2003–2010) along the U.S. west coast (Washington to California). *Deep Sea Research Part I: Oceanographic Research Papers*, *67*, 44–54. https://doi.org/10.1016/j.dsr.2012.05.002

Levin, L. A., Baco, A. R., Bowden, D. A., Colaco, A., Cordes, E. E., Cunha, M. R., Demopoulos, A. W. J., Gobin, J., Grupe, B. M., Le, J., Metaxas, A., Netburn, A. N., Rouse, G. W., Thurber, A. R., Tunnicliffe, V., Van Dover, C. L., Vanreusel, A., & Watling, L. (2016). Hydrothermal Vents and Methane Seeps: Rethinking the Sphere of Influence. *Frontiers in Marine Science*, *3*. https://doi.org/10.3389/fmars.2016.00072

Levin, L. A., James, D., Martin, C., Rathburn, A., Harris, L., & Michener, R. (2000). Do methane seeps support distinct macrofaunal assemblages? Observations on community structure and nutrition from the northern California slope and shelf. *Marine Ecology Progress Series*, *208*, 21–39. https://doi.org/10.3354/meps208021

Levin, L. A., Mendoza, G. F., Gonzalez, J. P., Thurber, A. R., & Cordes, E. E. (2010). Diversity of bathyal macrofauna on the northeastern Pacific margin: The influence of methane seeps and oxygen minimum zones. *Marine Ecology*, *31*(1), 94–110. https://doi.org/10.1111/j.1439-0485.2009.00335.x

Levin, L. A., & Michener, R. H. (2002). Isotopic evidence for chemosynthesis-based nutrition of macrobenthos: The lightness of being at Pacific methane seeps. *Limnology and Oceanography*, *47*(5), 1336–1345. https://doi.org/10.4319/lo.2002.47.5.1336

MacAvoy, S. E., Carney, R. S., Fisher, C. R., & Macko, S. A. (2002). Use of chemosynthetic biomass by large, mobile, benthic predators in the Gulf of Mexico. *Marine Ecology Progress Series*, *225*, 65–78. https://doi.org/10.3354/meps225065

Merle, S. G., Embley, R. W., Johnson, H. P., Lau, T.-K., Phrampus, B. J., Raineault, N. A., & Gee, L. J. (2021). Distribution of Methane Plumes on Cascadia Margin and Implications for the Landward Limit of Methane Hydrate Stability. *Frontiers in Earth Science*, *9*. https://doi.org/10.3389/feart.2021.531714

Muller-Karger, F. E., Varela, R., Thunell, R., Luerssen, R., Hu, C., & Walsh, J. J. (2005). The importance of continental margins in the global carbon cycle. *Geophysical Research Letters*, *32*(1). https://doi.org/10.1029/2004GL021346

Philip, B. T., Solomon, E. A., Kelley, D. S., Tréhu, A. M., Whorley, T. L., Roland, E., Tominaga, M., & Collier, R. W. (2023). Fluid sources and overpressures within the central Cascadia Subduction

Zone revealed by a warm, high-flux seafloor seep. *Science Advances*, *9*(4), eadd6688. https://doi.org/10.1126/sciadv.add6688

Prouty, N., Roark, E., Buster, N., & Ross, S. (2011). Growth rate and age distribution of deep-sea black corals in the Gulf of Mexico. *Marine Ecology Progress Series*, *423*, 101–115. https://doi.org/10.3354/meps08953

Ramirez-Llodra, E., Tyler, P. A., Baker, M. C., Bergstad, O. A., Clark, M. R., Escobar, E., Levin, L. A., Menot, L., Rowden, A. A., Smith, C. R., & Dover, C. L. V. (2011). Man and the Last Great Wilderness: Human Impact on the Deep Sea. *PLOS ONE*, *6*(8), e22588. https://doi.org/10.1371/journal.pone.0022588

Redmon, J., Divvala, S., Girshick, R., & Farhadi, A. (2016). You Only Look Once: Unified, Real-Time Object Detection. *2016 IEEE Conference on Computer Vision and Pattern Recognition (CVPR)*, 779–788. https://doi.org/10.1109/CVPR.2016.91

Riedel, M., Scherwath, M., Römer, M., Veloso, M., Heesemann, M., & Spence, G. D. (2018). Distributed natural gas venting offshore along the Cascadia margin. *Nature Communications*, *9*(1), 3264. https://doi.org/10.1038/s41467-018-05736-x

Rudebusch, J. A., Prouty, N. G., Conrad, J. E., Watt, J. T., Kluesner, J. W., Hill, J. C., Miller, N. C., Watson, S. J., & Hillman, J. I. T. (2023). Diving deeper into seep distribution along the Cascadia convergent margin, United States. *Frontiers in Earth Science*, *11*. https://doi.org/10.3389/feart.2023.1205211

Seabrook, S., C. De Leo, F., Baumberger, T., Raineault, N., & Thurber, A. R. (2018). Heterogeneity of methane seep biomes in the Northeast Pacific. *Deep Sea Research Part II: Topical Studies in Oceanography, Results of Telepresence-Enabled Oceanographic Exploration*, *150*, 195–209. https://doi.org/10.1016/j.dsr2.2017.10.016

Seabrook, S., De Leo, F. C., & Thurber, A. R. (2019). Flipping for Food: The Use of a Methane Seep by Tanner Crabs (Chionoecetes tanneri). *Frontiers in Marine Science*, *6*. https://doi.org/10.3389/fmars.2019.00043

Seabrook, S., Torres, M. E., Baumberger, T., Butterfield, D., Roe, K., Cummings, M., Crawford, R., & Thurber, A. R. (2024). Ubiquitous but unique: Water depth and oceanographic attributes shape methane seep communities. *Limnology and Oceanography*, *69*(5), 1218–1232. https://doi.org/10.1002/lno.12564

Suess, E. (2014). Marine cold seeps and their manifestations: Geological control, biogeochemical criteria and environmental conditions. *International Journal of Earth Sciences*, *103*(7), 1889–1916. https://doi.org/10.1007/s00531-014-1010-0

Suess, E., Torres, M. E., Bohrmann, G., Collier, R. W., Greinert, J., Linke, P., Rehder, G., Trehu, A., Wallmann, K., Winckler, G., & Zuleger, E. (1999). Gas hydrate destabilization: Enhanced dewatering, benthic material turnover and large methane plumes at the Cascadia convergent margin. *Earth and Planetary Science Letters*, *170*(1), 1–15. https://doi.org/10.1016/S0012-821X(99)00092-8

Teichert, B. M. A., Eisenhauer, A., Bohrmann, G., Haase-Schramm, A., Bock, B., & Linke, P. (2003). U/Th systematics and ages of authigenic carbonates from Hydrate Ridge, Cascadia Margin: Recorders of fluid flow variations. *Geochimica et Cosmochimica Acta*, *67*(20), 3845–3857. https://doi.org/10.1016/S0016-7037(03)00128-5

Thurber, A. R., Sweetman, A. K., Narayanaswamy, B. E., Jones, D. O. B., Ingels, J., & Hansman, R. L. (2014). Ecosystem function and services provided by the deep sea. *Biogeosciences*, *11*(14), 3941–3963. https://doi.org/10.5194/bg-11-3941-2014

Treude, T., Boetius, A., Knittel, K., Wallmann, K., & Jørgensen, B. B. (2003). Anaerobic oxidation of methane above gas hydrates at Hydrate Ridge, NE Pacific Ocean. *Marine Ecology Progress Series*, *264*, 1–14. https://doi.org/10.3354/meps264001

Wagner, J. K. S., McEntee, M. H., Brothers, L. L., German, C. R., Kaiser, C. L., Yoerger, D. R., & Van Dover, C. L. (2013). Cold-seep habitat mapping: High-resolution spatial characterization of the Blake Ridge Diapir seep field. *Deep Sea Research Part II: Topical Studies in Oceanography, Deep-Sea Biodiversity and Life History Processes*, *92*, 183–188. https://doi.org/10.1016/j.dsr2.2013.02.008

Zatsepina, O. Ye., & Buffett, B. A. (1997). Phase equilibrium of gas hydrate: Implications for the formation of hydrate in the deep sea floor. *Geophysical Research Letters*, *24*(13), 1567–1570. https://doi.org/10.1029/97GL01599